AGU PUBLICATIONS

Geophysical Research Letters

RESEARCH LETTER
10.1002/2016GL068359

Special Section:
First results from NASA's Magnetospheric Multiscale (MMS) Mission

Currents and associated electron scattering and bouncing near the diffusion region at Earth's magnetopause

B. Lavraud[1,2], Y. C. Zhang[1,2,3], Y. Vernisse[1,2], D. J. Gershman[4,5], J. Dorelli[4], P. A. Cassak[6], J. Dargent[1,2,7], C. Pollock[4], B. Giles[4], N. Aunai[7], M. Argall[8], L. Avanov[4,5], A. Barrie[4,9], J. Burch[10], M. Chandler[11], L.-J. Chen[4], G. Clark[12], I. Cohen[12], V. Coffey[11], J. P. Eastwood[13], J. Egedal[14], S. Eriksson[15], R. Ergun[15], C. J. Farrugia[8], S. A. Fuselier[10], V. Génot[1,2], D. Graham[16], E. Grigorenko[17], H. Hasegawa[18], C. Jacquey[1,2], I. Kacem[1,2], Y. Khotyaintsev[16], E. MacDonald[4], W. Magnes[19], A. Marchaudon[1,2], B. Mauk[12], T. E. Moore[4], T. Mukai[18], R. Nakamura[19], W. Paterson[4], E. Penou[1,2], T. D. Phan[20], A. Rager[4,21], A. Retino[7], Z. J. Rong[22], C. T. Russell[23], Y. Saito[18], J.-A. Sauvaud[1,2], S. J. Schwartz[13,15], C. Shen[24], S. Smith[4,21], R. Strangeway[23], S. Toledo-Redondo[25], R. Torbert[8], D. L. Turner[26], S. Wang[9], and S. Yokota[18]

[1]Institut de Recherche en Astrophysique et Planétologie, Université de Toulouse, Toulouse, France, [2]Centre National de la Recherche Scientifique, UMR 5277, Toulouse, France, [3]State Key Laboratory of Space Weather, NSSC/CAS, Beijing, China, [4]NASA Goddard Space Flight Center, Greenbelt, Maryland, USA, [5]Department of Astronomy, University of Maryland, College Park, Maryland, USA, [6]Department of Physics and Astronomy, West Virginia University, Morgantown, West Virginia, USA, [7]Laboratoire de Physique des Plasmas, Palaiseau, France, [8]Physics Department, University of New Hampshire, Durham, New Hampshire, USA, [9]Millenium Engineering and Integration Company, Arlington, Virginia, USA, [10]Southwest Research Institute, San Antonio, Texas, USA, [11]NASA Marshall Space Flight Center, Huntsville, Alabama, USA, [12]The Johns Hopkins University Applied Physics Laboratory, Laurel, Maryland, USA, [13]The Blackett Laboratory, Imperial College, London, UK, [14]Department of Physics, University of Wisconsin, Madison, Wisconsin, USA, [15]Laboratory for Atmospheric and Space Physics, University of Colorado Boulder, Boulder, Colorado, USA, [16]Swedish Institute of Space Physics, Uppsala, Sweden, [17]Space Research Institute of the Russian Academy of Sciences, Moscow, Russia, [18]Institute of Space and Astronautical Science, JAXA, Sagamihara, Japan, [19]Space Research Institute, Austrian Academy of Sciences, Graz, Austria, [20]Space Sciences Laboratory, Berkeley, California, USA, [21]Department of Physics, Catholic University of America, Washington, District of Columbia, USA, [22]Key Laboratory of Earth and Planetary Physics, IGG/CAS, Beijing, China, [23]Department of Earth and Space Sciences, University of California, Los Angeles, California, USA, [24]Harbin Institute of Technology, Shenzhen, China, [25]ESAC/ESA, Villafranca del Castillo, Spain, [26]The Aerospace Corporation, El Segundo, California, USA

Abstract Based on high-resolution measurements from NASA's Magnetospheric Multiscale mission, we present the dynamics of electrons associated with current systems observed near the diffusion region of magnetic reconnection at Earth's magnetopause. Using pitch angle distributions (PAD) and magnetic curvature analysis, we demonstrate the occurrence of electron scattering in the curved magnetic field of the diffusion region down to energies of 20 eV. We show that scattering occurs closer to the current sheet as the electron energy decreases. The scattering of inflowing electrons, associated with field-aligned electrostatic potentials and Hall currents, produces a new population of scattered electrons with broader PAD which bounce back and forth in the exhaust. Except at the center of the diffusion region the two populations are collocated and appear to behave adiabatically: the inflowing electron PAD focuses inward (toward lower magnetic field), while the bouncing population PAD gradually peaks at 90° away from the center (where it mirrors owing to higher magnetic field and probable field-aligned potentials).

Key Points:
- Observation of Hall current-associated electron dynamics near the diffusion region
- Confirmation of low-energy electron scattering by curved magnetic field lines
- Simultaneous observation of inflowing and outflowing, bouncing populations

Supporting Information:
- Supporting Information S1

Correspondence to:
B. Lavraud,
Benoit.Lavraud@irap.omp.eu

Citation:
Lavraud, B., et al. (2016), Currents and associated electron scattering and bouncing near the diffusion region at Earth's magnetopause, *Geophys. Res. Lett.*, *43*, 3042–3050, doi:10.1002/2016GL068359.

Received 19 FEB 2016
Accepted 22 MAR 2016
Accepted article online 28 MAR 2016
Published online 6 APR 2016

1. Introduction

The process of magnetic reconnection is ubiquitous in the plasma universe. Although it has major large-scale implications on the surrounding media, the key processes that drive magnetic reconnection occur at very small scales in a region known as the diffusion region (where magnetic fields diffuse and reconnect with a new topology) [e.g., *Priest and Forbes*, 2000]. In proton-electron plasmas, as observed near Earth, for instance, the vastly different particle masses lead to a structured region wherein the ions (with larger gyroradius) decouple from the magnetic field farther from the X line (where the topology changes) than electrons. This separation leads to the formation of an ion diffusion region with characteristic Hall currents and magnetic fields embedding a much smaller electron diffusion region [e.g., *Øieroset et al.*, 2001; *Mozer et al.*, 2002]. While missions such as the

multispacecraft Cluster mission have instrumentation and interspacecraft separation on the order of the typical ion scales at Earth's magnetopause, the recently launched Magnetospheric Multiscale (MMS) mission has been designed to measure the details of electron dynamics to understand electron-scale physics in the vicinity of these diffusion regions [*Burch et al.*, 2015].

Electron dynamics in collisionless magnetic reconnection has been studied mostly using test particle [*Speiser*, 1965] and particle-in-cell simulations [e.g., *Hoshino et al.*, 2001; *Fu et al.*, 2006; *Pritchett*, 2006; *Drake et al.*, 2008; *Wan et al.*, 2008; *Hesse et al.*, 2014]. For the present study, of particular interest is the prediction that particle pitch angle scattering should occur when the gyroradius of a particle is on the order of the scale of the local magnetic field curvature. With R_c the local magnetic field curvature and R_g the particle gyroradius, one can define an adiabatic parameter κ by $\kappa^2 = R_c/R_g$. Based on this parameter, theory predicts that particle scattering (of ions or electrons) occurs when κ^2 approaches 25 and that particle dynamics becomes chaotic for values below 10 [*Sergeev et al.*, 1983; *Büchner and Zelenyi*, 1989; *Young et al.*, 2008]. Observations of proton dynamics in the radiation belts and ring current have, for instance, been attributed to scattering by curved magnetic field configurations [*Zou et al.*, 2011; *Shen et al.*, 2014]. Regarding electrons, simulations have mostly been used to study their dynamics in the vicinity of magnetic reconnection regions, with more chaotic behaviors identified near the X line where the local magnetic field line curvature becomes comparable to the electron gyroradius [e.g., *Wang et al.*, 2010]. In the magnetotail ion diffusion region, isotropic electron observations at energies of a few keV were explained by local electric fields and magnetic curvature pitch angle scattering [*Egedal et al.*, 2005; *Wang et al.*, 2010]. Although recent theory and numerical modeling have predicted complex behaviors at electron scales as well [*Ng et al.*, 2011, 2012; *Bessho et al.*, 2014, 2015; *Haggerty et al.*, 2015; *Wang et al.*, 2016], no appropriate spacecraft observations have been available. The present paper is devoted to novel observations of currents in the Hall region and associated electron demagnetization, scattering and bouncing down to the smallest scales near the diffusion region, which will contribute to our understanding of the fine structure and dynamics of magnetic reconnection.

2. Mission and Instrumentation

The four NASA MMS [*Burch et al.*, 2015] spacecraft were launched together on 12 March 2015 on an Atlas V launch vehicle into a highly elliptical 28° inclination orbit with perigee at 1.2 Earth radii (R_E) and apogee at 12 R_E. The main requirements for the mission objectives were the following: (1) four spacecraft in a close tetrahedron formation with adjustable separations down to 10 km, (2) accurate three-axis electric and magnetic field measurements for estimating spatial gradients and time variations, and (3) three-dimensional electron and ion distribution functions at the highest time resolution ever achieved (30 ms for electrons and 150 ms for ions). For the present paper, we primarily focus on ion and electron measurements from the Fast Plasma Instruments [*Pollock et al.*, 2016] and magnetic field measurements from the fluxgate magnetometers [*Russell et al.*, 2015]. We primarily show data from the MMS4 spacecraft, except when using multispacecraft methods or measurements as stated in the text.

3. Diffusion Region Observations

To study the current systems and the occurrence of electron pitch angle scattering and bouncing in the vicinity of the diffusion region of magnetic reconnection, the magnetopause crossings of 3 October 2015 (near 14:07:00 UT) and 16 October 2015 (near 10:33:30 UT) are presented in Figure 1. The figure shows the former event in Figures 1a–1h and the latter in Figures 1i–1p. For the events, we perform a minimum variance analysis [*Sonnerup and Scheible*, 1998] on the intervals 14:46:58–14:47:03 UT and 10:33:22–10:33:37 UT, respectively, which is used to transform the ion velocities and magnetic fields in Figures 1d and 1f into boundary normal LMN coordinates (where N points outward into the magnetosheath and L has a positive Z_{GSE} component). Figures 2a and 2b display the out-of-plane (Hall) magnetic field and the parallel currents, respectively, from a full particle-in-cell simulation performed for typical asymmetric magnetopause conditions. These simulation figures are merely used here for illustration purposes, but their description is given in the associated supporting information for completeness. The notional virtual spacecraft trajectory in the vicinity of the X line is depicted for the two events in Figure 2a based on the following description.

Figures 1a–1h from 3 October 2015 display the typical signatures of the crossing of an ion diffusion region, i.e., with Hall magnetic field (B_M) and current signatures. The region labeled 1 in Figure 1d for this event shows a

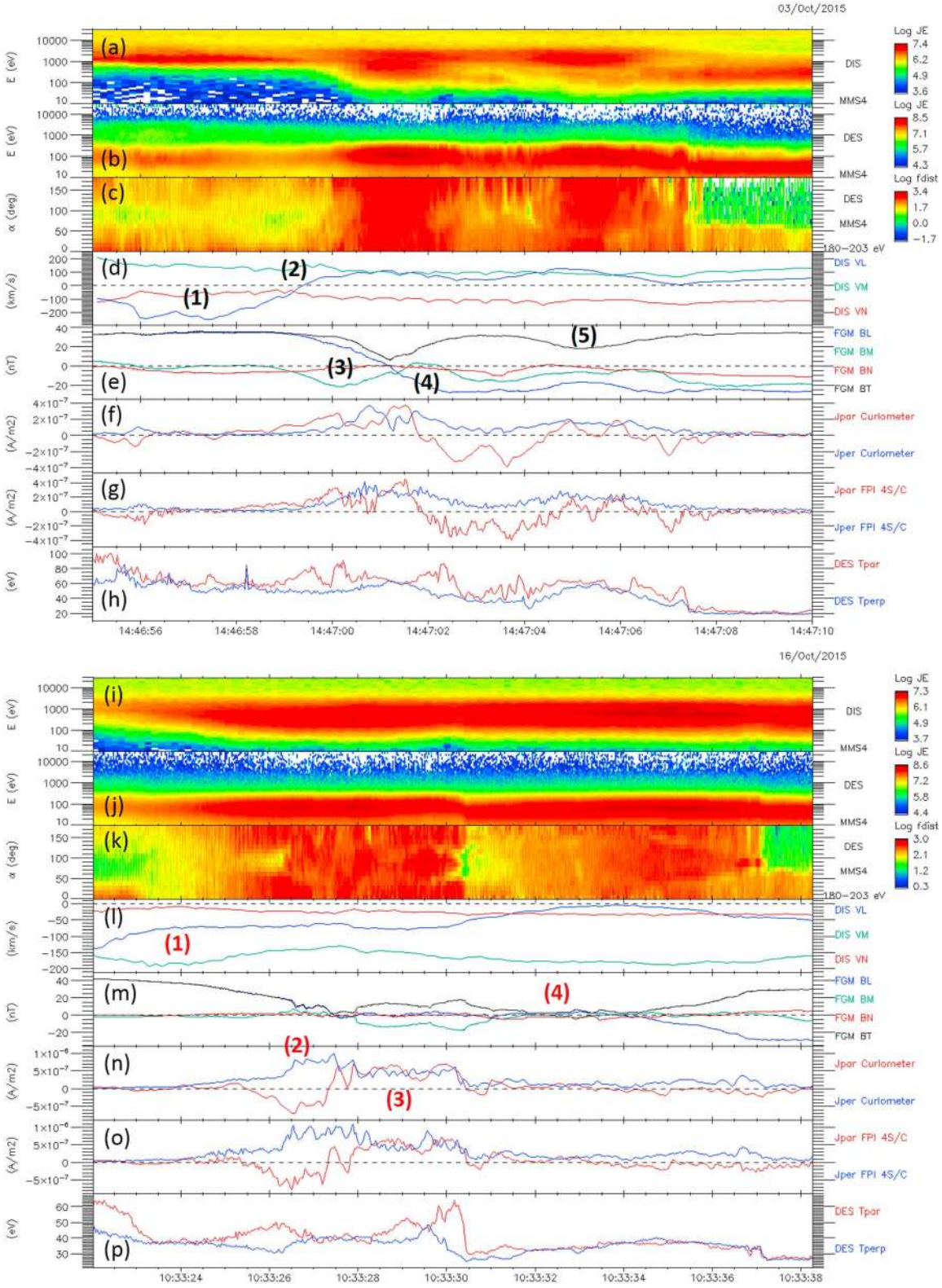

Figure 1. MMS plasma and magnetic field observations from two ion diffusion region crossings (3 October 2015 and 16 October 2015). (a–h) The ion energy-time spectrogram, electron energy-time spectrogram, 200 eV electron PAD spectrogram, ion velocity and magnetic field components in LMN coordinates, the parallel and perpendicular currents from the four-spacecraft Curlometer method (Figure 1f) and from the particles measurements (Figure 1g; average of the currents from the four spacecraft), and finally the parallel and perpendicular electron temperatures (Figure 1h). (i–p) The same but for the second event on 16 October 2015. Several key regions, as identified in the text, are numbered in black and red for each event. These regions are also reported in the simulation illustration in Figure 2a.

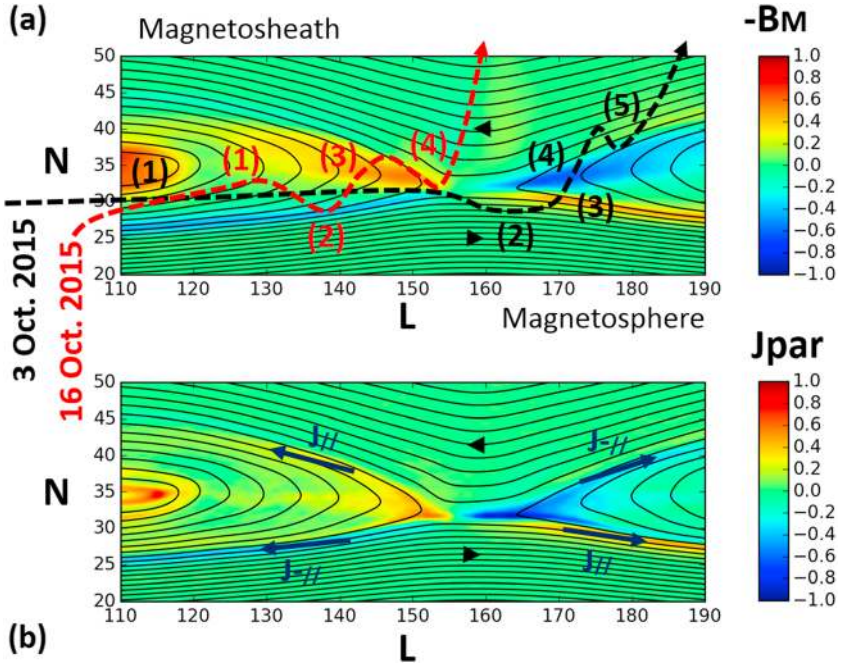

Figure 2. (a) The out-of-plane Hall B_M magnetic field component and parallel component of the currents with overlaid magnetic field lines in black from a particle-in-cell simulation described in the supporting information. The parallel currents are related to parallel electrostatic potentials, while perpendicular currents drive the classic out-of-plane Hall magnetic field signature of Figure 2a. The notional relative spacecraft paths for the two events, with various identified regions numbered as described in the text, are shown in these simulation plots for illustration purposes only. The properties of the parallel currents are sketched in Figure 2b.

negative V_L component, consistent with the location of region 1 for this event as shown in Figure 2a along the black dashed arrow displaying the spacecraft trajectory. Going forward in time for this event, region 2 corresponds to the passage from the left-hand side of the X line to its right-hand side, so that region 2 is where V_L switches sign to a positive value. The spacecraft then enters the negative B_M Hall magnetic field in region 3 and exits the region through the opposite polarity Hall magnetic field in region 4 (positive B_M in Figure 1e). A short time later the satellite returns to the positive Hall magnetic field region (region 5). After region 5, the satellite exits into the magnetosheath, characterized by a large southward magnetic field, consistent with the crossing of an ion diffusion region at a reconnecting, large magnetic shear magnetopause.

The Hall magnetic field signatures are confirmed by the independent calculations of the currents based on the multispacecraft curlometer method [*Robert et al.*, 1998] in Figure 1f and the direct particle measurements in Figure 1g, i.e., $\boldsymbol{J} = Nq(\boldsymbol{V_i} - \boldsymbol{V_e})$ (where $\boldsymbol{J}$ is the current density vector, N is the plasma density, q is the electric charge, and $\boldsymbol{V_i}$ and $\boldsymbol{V_e}$, respectively, are the ion and electron velocity vectors). The current from particle measurements in Figure 1g is the average over the four spacecraft individual measurements and is thus directly comparable with that estimated from the curlometer over the tetrahedron (note that for the two events studied the interspacecraft separation is on the order of 10 km). Only the parallel and perpendicular currents are displayed for more direct comparison with the simulation results in Figures 2a and 2b. As can be seen, these two independent measures of the currents match each other extremely well, demonstrating the unprecedented level of accuracy in particle measurements reached by MMS.

Strong perpendicular currents consistent with the Hall currents are observed throughout the region containing the out-of-plane B_M magnetic field signature. Strong parallel currents are also measured as the spacecraft crosses the Hall region. The parallel current changes sign across the midplane (where B_Z changes sign), consistent with outward flowing currents and with strong inward acceleration of field-aligned electrons. This acceleration is most likely the result of field-aligned potentials accelerating electrons inward [*Egedal et al.*, 2005, 2008] but may also be involving Fermi-type acceleration [e.g., *Drake et al.*, 2009]. These observations are also consistent with the increased parallel electron temperature observed at the edges of the exhaust in Figure 1h, as also observed from simulations [*Le et al.*, 2010; *Wang et al.*, 2016]. More intermixed

parallel and perpendicular components of the currents are measured in the center of the region. Analysis of the detailed interplay between various processes in this complex current system is left for future work.

Of specific interest for the present study is Figure 1c, which shows the pitch angle distribution (PAD) of 200 eV electrons. While these electrons show clear anisotropies in the magnetosphere (bidirectional to the left) and magnetosheath (unidirectional at 0° to the right), in the identified ion diffusion region these 200 eV electrons appear much more isotropic. This is also observed in measured electron temperatures in Figure 1h.

To further quantify the properties of this crossing, we used a multispacecraft timing method [e.g., *Russell et al*., 1983] to determine the magnetopause normal direction—based on the B_Z component reversal (zero crossing times)—which we found as $(0.90; 0.36; -0.24)_{GSE}$ with a normal speed of 65 km/s. Given a full diffusion region duration of about 3 s, the spatial thickness of the region is 195 km. With a density of 12 cm^{-3} as observed just outside in the magnetosheath (not shown), the typical ion skin depth λ_i is estimated as 66 km. The ion diffusion region thickness is thus about $3\lambda_i$. Assuming fast reconnection with a diffusion region aspect ratio of 0.1 (ratio of the thickness to width of the region), the crossing distance to the X line is estimated as $15\lambda_i$ (or ~987 km), as roughly represented by the spacecraft trajectory in Figure 2a.

A similar overview of the 16 October event is now described based on Figures 1i–1p. The spacecraft sampling of the X line vicinity is illustrated with the red dashed arrow in the simulation plot of Figure 2b. As with the first event, the magnetopause crossing starts on the magnetospheric side with a negative V_L components (region 1 in Figures 1l and 2b). Unlike the first event, however, the spacecraft does not cross to the other side of the X line, as shown by the continuously $-V_L$ component throughout the event (Figure 1l), and the consistently reversed polarity (compared to the first event) of the Hall magnetic field and currents (Figures 1m–1o), identified as regions 2 and 3. Note that the positive Hall B_M upon entry is rather weak in the present event, but such asymmetry is not unusual at the asymmetric magnetopause [*Mozer et al*., 2008]. For this event again the currents are independently and accurately estimated by the curlometer and particle measurements, with parallel and perpendicular components consistent with expectations from previous work and simulations (Figure 2b). As for the first event, strong parallel currents and enhanced (parallel) temperature anisotropy are observed at the edges of the exhaust, suggestive of parallel electrostatic potentials and Fermi acceleration.

After region 3, the spacecraft does not exit into the magnetosheath but apparently comes back toward the magnetopause (region 4) before a final exit at 10:33:37 UT. Given the particularly low magnetic field and the absence of a strong Hall magnetic field signature in region 4, it is possible that the spacecraft approaches the electron diffusion region during this period. This is also confirmed by the estimation of the distance to the X line: 6.5 ion skin depths. This estimation was performed as for the first event using a normal vector $(0.92; 0.02; -0.4)_{GSE}$ from multispacecraft timing, a normal speed of 12 km/s, and a magnetosheath density of 20 cm^{-3}. Note that given the proximity to the X line, the determination of the timing was complex in this case. The estimated normal speed likely varies over time as exemplified by the second reentry into the diffusion region, for instance.

Whether the event of 16 October 2015 is an actual electron diffusion region is not addressed further here, as the focus of the present paper is on current systems and electron pitch angle scattering and bouncing in the vicinity of this region, rather than in specifically studying the electron diffusion region. The reader is referred to ongoing MMS studies on this topic which will soon be published. As further detailed in section 4, Figure 1k shows again enhanced isotropy in the 200 eV electron PAD in the identified diffusion region as compared to the surrounding magnetospheric and magnetosheath electron populations (which are again, respectively, bidirectional and unidirectional at this energy).

4. Electron Focusing and Bouncing in the Hall Region

The event on 3 October 2015 above was presented first as a textbook case of ion diffusion region crossing and to highlight the observation of broader PAD at various distances from the X line. Now we focus on the more detailed observation of electron focusing and bouncing in the vicinity of the X line based on the 16 October 2015 event. This event is chosen for more detailed analysis because the spacecraft likely approached closer to the X line on that day than on 3 October 2015, and the slow crossing (cf. section 3) better emphasizes key transitions, namely, (1) the gradual focusing and bouncing of electrons and (2) the spatial separation of the scattering as a function of electron energy.

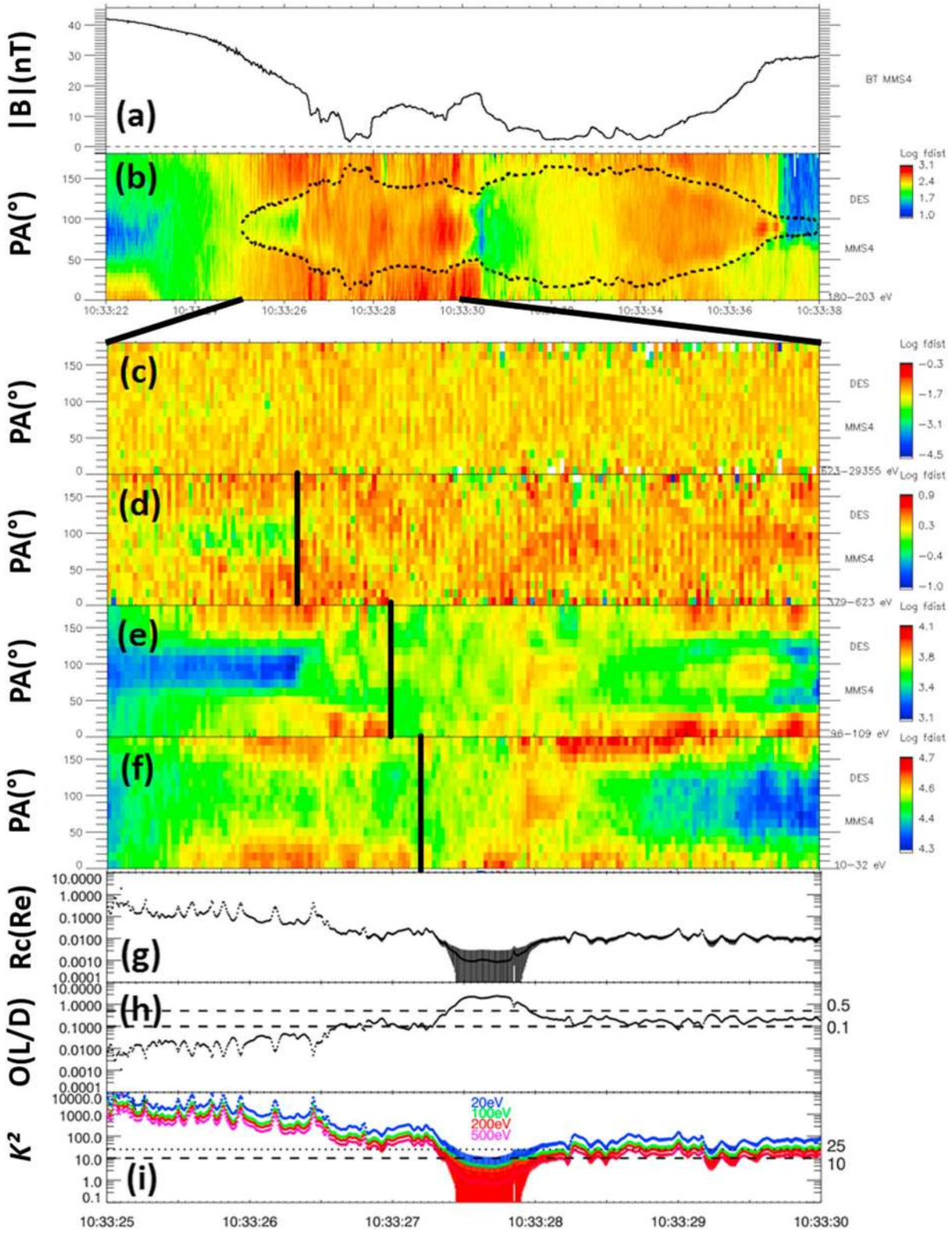

Figure 3. MMS observations zoomed on an interval of interest during the event of 16 October 2015. (a) The magnetic field magnitude and (b) the 200 eV electron PAD. Figure 3b also shows with a thick dashed line the pitch angle focusing expected from adiabatic behavior (cf. text for details). (c–f) PAD spectrograms at four electron energies of about >600 eV, 400 eV, 100 eV, and 20 eV. The thick vertical lines mark the passage from an anisotropic population (peaked at 0° and/or 180°) to an isotropic population for each energy. (g–i) The magnetic field radius of curvature, the error associated with the method, and the adiabatic parameter κ^2 for four different energies based on the results of a magnetic curvature analysis (MCA; cf. text and supporting information for details).

Figure 3a shows the magnetic field strength, while Figure 3b displays the PAD for electrons at 200 eV for the interval of interest on 16 October 2015. As mentioned previously, while these 200 eV electrons show clear anisotropies at the beginning of the interval (in the magnetosphere) and at the end of the interval (in the magnetosheath), much more isotropic PADs are observed in the low magnetic field regions. Superimposed on the electron PAD spectrogram we show with a thick dashed line the expected narrowing/broadening of both field-aligned and anti–field-aligned electron populations as a function of magnetic field strength assuming conservation of the first adiabatic invariant. We take for this purpose an outer magnetic field strength of 30 nT (chosen to best match the observed pitch angle focusing), which we consider as a mirror point ($\mathbf{B}_{MIRROR}$; this corresponds to where the dashed line ends on the left-hand side), and calculate the expected focusing/broadening of an adiabatic electron population as follows: $\alpha = \sin^{-1}(\sqrt{(|\mathbf{B}|/|\mathbf{B}_{MIRROR}|)})$. The dashed line shows that field-aligned and anti–field-aligned electrons follow the expected focusing/broadening. Going forward in time from the left-hand side of the dashed line, however, a new electron population centered on 90° pitch angle appears at 10:33:26.5 UT. This population gradually broadens as the magnetic field magnitude decreases. A faint demarcation (slightly lower fluxes) between this population and the more field-aligned population is observed throughout the event. This demarcation is particularly clear in the interval 10:33:34–10:33:37 UT, for instance. This latter interval is remarkable for demonstrating that in fact, the pitch angle extent of both the (anti–)field-aligned and 90°-centered populations follow the thick dashed line. Thus, the broad, nearly isotropic population observed in the regions of lowest magnetic field strength also obeys an adiabatic behavior. It gradually peaks and thus mirrors at 90° pitch angle, as the electrons try to exit the low magnetic field region. This population is thus bouncing (quasi-trapped) in the low magnetic field region near the X line in the ion diffusion region. Given the expected topology in the vicinity of an X line, the 90°-centered population is only quasi-trapped because it will eventually convect away from the X line vicinity where the magnetic field typically does not show as prominent magnetic field minima (so this population cannot remain trapped indefinitely as reconnected field lines propagate in the outflow direction).

Our interpretation of the above observations is as follows. The out-of-plane B_M magnetic field signature is induced by the observed perpendicular Hall currents throughout the region. The field-aligned and anti–field-aligned populations just outside the lowest magnetic field region correspond to those carrying the outward field-aligned currents measured at the edges of the region (with enhanced parallel temperatures). These strong parallel currents may result from combined field-aligned electrostatic potentials and Fermi-type acceleration. This is supported by increased parallel electron temperatures at these locations and past simulations. Estimates of the parallel electrostatic potentials are, however, left for future work. The inflowing population gets more and more focused along the magnetic field that threads the diffusion region as the magnetic field strength decreases. The appearance of the 90°-peaked population (e.g., 10:33:26.5 or 10:30:37.0 UT) is interpreted, on the other hand, as a locally mirroring population which comes from near the vicinity of the X line or main current sheet where the magnetic field strength is very low but the magnetic field curvature very high. Scattering, and possibly additional energization, of the field-aligned electrons is thus expected to occur close to the X line and main current sheet. The electrons scattered there are able to travel outward some distance along the magnetic field before mirroring back toward the X line. They bounce back and forth as long as a sufficient magnetic field minimum or parallel electrostatic potential remains in the vicinity of the main current sheet. This explains both the colocation of the two electron populations and their adiabatic behavior (PADs "bordered" by the thick dashed line) in the Hall region where they are largely magnetized. The bouncing mechanisms (adiabatic mirroring and parallel potentials) and pitch angle observations suggest the existence of a loss-cone effect whereby only part of the initially scattered distribution function (nonparallel electrons) can be trapped while parallel electrons are lost along the field lines.

5. Electron Scattering in Highly Curved Magnetic Field Lines

We now focus on a more detailed investigation of where and how the scattering occurs. Figures 3c–3i show MMS data zoomed on the first entry into the ion diffusion region for the 16 October 2015 event. The four first panels (Figures 3a–3d) show electron PADs at four different energies (>600 eV, 500 eV, 100 eV, and 20 eV). The next panels (Figures 3g–3i) show the results of a Magnetic Curvature Analysis (MCA) performed on this interval, the details of which are presented in *Shen et al*. [2003] and in the supporting information associated with this paper. The errors related with the method have been shown to be on the order of the ratio of the

spatial scale of the tetrahedron (spacecraft separation of order ~10 km for this event) to the spatial scale of the structure (here the local magnetic field curvature radius). It should be noted that the MCA has been used in many previous studies and has shown its ability to produce meaningful curvature estimates at all scales that could be reached with past missions: current sheets and plasmoids [*Shen et al.*, 2008; *Rong et al.*, 2011; *Zhang et al.*, 2013; *Yang et al.*, 2014], as well as larger scale structures such as the ring current [*Shen et al.*, 2014].

As introduced previously, theory [*Büchner and Zelenyi*, 1989] predicts that particle scattering occurs when κ^2 nears 25 and that the particle dynamics becomes chaotic for values below 10. Figure 3g shows the expected high curvature in the lowest magnetic field region, as estimated from the MCA. Figure 3h shows the errors, which are also reported in Figures 3g and 3i and increase as expected in the region of increased curvature. Despite large errors, the scale of the MMS tetrahedron is sufficiently small to study the magnetic field curvature down to the scale of low energy electrons. This is demonstrated in Figure 3i where the κ^2 value for five electron energies are shown. These energies correspond to those shown in the PAD spectrograms of Figures 3c–3f (apart from 200 eV, for which the PAD is similar to that at 100 eV). Thick vertical black lines are shown in the PAD for each energy, except for the highest energy where no distinction can be made regarding the anisotropy owing in part to low count rates. Going forward in time from the left, these vertical lines show the time at which anisotropic distributions with primarily field-aligned and anti–field-aligned populations disappear, or in other words where these electrons have been scattered (in angles and possibly also in energy) to other parts of velocity space. These vertical lines roughly correspond to the times at which the colored curves (for each energy) in Figure 2i start to approach a κ^2 value of 25, as predicted by theory for pitch angle scattering in curved magnetic field lines. Near the center of the region with the lowest magnetic field and highest curvature, electrons at all energies appear scattered and much more isotropic than at other times.

As can be seen for the 100 eV and 200 eV populations (Figures 3e and 3b), the time at which the field-aligned population is scattered is later, i.e., closer to the X line or current sheet, than the time at which the broader population peaks at 90°. This confirms the interpretation of section 4 that while scattering occurs close to the X line, parts of the scattered electrons bounce back and forth in the outflow region and mirror at significant distances so that a large part of the Hall region contains both populations simultaneously (both contribute to the parallel/perpendicular current structure of the ion diffusion region). These high-resolution electron observations bear a strong resemblance with recent simulation results [e.g., *Ng et al.*, 2011; *Bessho et al.*, 2014, 2015; *Haggerty et al.*, 2015; *Egedal et al.*, 2015; *Wang et al.*, 2016].

6. Conclusions

Thanks to unprecedented high-resolution electron measurements from NASA's MMS mission, the intricate dynamics of electron populations and associated currents in the vicinity of the diffusion region of magnetic reconnection at Earth's dayside magnetopause are revealed. We have shown that electrons are scattered most likely by the highly curved geometry of the magnetic field lines in this region. This was demonstrated by the scattering being observed closer to the X line as the energy of electrons decreases. With the small separation of the MMS spacecraft, the local magnetic field curvature could be studied down to the electron scale and down to energies as low as 20 eV. We showed that the scattering process, combined with trapping mechanisms, leads to the superposition of two electron populations in parts of the Hall region: one inflowing population (carrying outward field-aligned currents likely related to parallel electrostatic potentials and Fermi acceleration) whose PAD width focuses as it approaches the main current sheet with lower magnetic field, and one outflowing population, whose source is the inflowing population that has been scattered closer to the X line or current sheet and then bounced back and forth in the magnetic field minimum of the ion diffusion region and exhaust. This second population can reach the observing point, away from its scattering location, as long as it is not forced to mirror back. The mirroring is observed as a gradual peaking toward 90° pitch angle away from the magnetic field minimum and is expected to result from both adiabatic mirroring in stronger magnetic field and trapping by parallel electrostatic potentials. We finally stress that while the present study shows a strong relation between electron scattering and magnetic field line curvature, future studies ought to investigate the relative role of electric fields and waves for a more complete description of electron dynamics. These novel electron-scale observations have broad impact on our current understanding of the fine structure of plasma populations in the vicinity of the reconnection region, in particular with regard to magnetic reconnection theory and numerical modeling.

Acknowledgments
For MMS data, visit https://lasp.colorado.edu/mms/sdc/public/. We thank all the MMS teams for their remarkable work and great hardware accomplishments. Work at IRAP was performed with the support of CNRS and CNES. The authors would like to thank the SMILEI development team for their support and providing them with the code SMILEI. S.J.S. thanks the Leverhulme Trust for its award of a Research Fellowship.

References

Bessho, N., L.-J. Chen, J. R. Shuster, and S. Wang (2014), Electron distribution functions in the electron diffusion region of magnetic reconnection: Physics behind the fine structures, *Geophys. Res. Lett.*, *41*, 8688–8695, doi:10.1002/2014GL062034.

Bessho, N., L.-J. Chen, K. Germaschewski, and A. Bhattacharjee (2015), Electron acceleration by parallel and perpendicular electric fields during magnetic reconnection without guide field, *J. Geophys. Res. Space Physics*, *120*, 9355–9367, doi:10.1002/2015JA021548.

Büchner, J., and L. M. Zelenyi (1989), Regular and chaotic charged particle motion in magnetotail-like field reversals: 1. Basic theory of trapped motion, *J. Geophys. Res.*, *94*(A9), 11,821–11,842, doi:10.1029/JA094iA09p11821.

Burch, J. L., T. E. Moore, R. B. Torbert, and B. L. Giles (2015), Magnetospheric multiscale overview and science objectives, *Space Sci. Rev.*, 1–17, doi:10.1007/s11214-015-0164-9.

Drake, J. F., M. A. Shay, and M. Swisdak (2008), The Hall fields and fast magnetic reconnection, *Phys. Plasmas*, *15*, 042,306.

Drake, J. F., M. Swisdak, T. D. Phan, P. A. Cassak, M. A. Shay, S. T. Lepri, R. P. Lin, E. Quataert, and T. H. Zurbuchen (2009), Ion heating resulting from pickup in magnetic reconnection exhausts, *J. Geophys. Res.*, *114*, A05111, doi:10.1029/2008JA013701.

Egedal, J., M. Øieroset, W. Fox, and R. P. Lin (2005), In situ discovery of an electrostatic potential, trapping electrons and mediating fast reconnection in the Earth's magnetotail, *Phys. Rev. Lett.*, *94*, 025006.

Egedal, J., W. Fox, N. Katz, M. Porkolab, M. Øieroset, R. P. Lin, W. Daughton, and J. F. Drake (2008), Evidence and theory for trapped electrons in guide field magnetotail reconnection, *J. Geophys. Res.*, *113*, A12207, doi:10.1029/2008JA013520.

Egedal, J., W. Daughton, A. Le, and A. L. Borg (2015), Double layer electric fields aiding the production of energetic flat-top distributions and superthermal electrons within magnetic reconnection exhausts, *Phys. Plasmas*, *22*, 101208.

Fu, X. R., Q. M. Lu, and S. Wang (2006), The process of electron acceleration during collisionless magnetic reconnection, *Phys. Plasmas*, *13*, 012309.

Haggerty, C. C., M. A. Shay, J. F. Drake, T. D. Phan, and C. T. McHugh (2015), The competition of electron and ion heating during magnetic reconnection, *Geophys. Res. Lett.*, *42*, 9657–9665, doi:10.1002/2015GL065961.

Hesse, M., N. Aunai, D. Sibeck, and J. Birn (2014), On the electron diffusion region in planar, asymmetric, systems, *Geophys. Res. Lett.*, *41*, 8673–8680, doi:10.1002/2014GL061586.

Hoshino, H., T. Mukai, T. Terasawa, and I. Shinohara (2001), Suprathermal electron acceleration in magnetic reconnection, *J. Geophys. Res.*, *106*, 25,979–25,997, doi:10.1029/2001JA900052.

Le, A., J. Egedal, W. Daughton, J. Drake, W. Fox, and N. Katz (2010), Magnitude of the Hall fields during magnetic reconnection, *Geophys. Res. Lett.*, *37*, L03106, doi:10.1029/2009GL041941.

Mozer, F. S., S. D. Bale, and T. D. Phan (2002), Evidence of diffusion regions at a subsolar magnetopause crossing, *Phys. Rev. Lett.*, *89*, 015002.

Mozer, F. S., V. Angelopoulos, J. Bonnell, K. H. Glassmeier, and J. P. McFadden (2008), THEMIS observations of modified Hall fields in asymmetric magnetic field reconnection, *Geophys. Res. Lett.*, *35*, L17S04, doi:10.1029/2007GL033033.

Ng, J., J. Egedal, A. Le, W. Daughton, and L.-J. Chen (2011), Kinetic structure of the electron diffusion region in antiparallel magnetic reconnection, *Phys. Rev. Lett.*, *106*, 065002, doi:10.1103/PhysRevLett.106.065002.

Ng, J., J. Egedal, A. Le, and W. Daughton (2012), Phase space structure of the electron diffusion region in reconnection with weak guide fields, *Phys. Plasmas*, *19*, 112108, doi:10.1063/1.4766895.

Øieroset, M., T. D. Phan, M. Fujimoto, R. P. Lin, and R. P. Lepping (2001), In situ detection of collisionless reconnection in the Earth's magnetotail, *Nature*, *412*, 414–417.

Pollock, C., et al. (2016), Fast plasma investigation for magnetospheric multiscale, *Space Sci. Rev.*, doi:10.1007/s11214-016-0245-4.

Priest, E., and T. Forbes (2000), *Magnetic Reconnection: MHD Theory and Applications*, Cambridge Univ. Press, Cambridge, U. K.

Pritchett, P. L. (2006), Relativistic electron production during driven magnetic reconnection, *Geophys. Res. Lett.*, *33*, L13104, doi:10.1029/2005GL025267.

Robert, P., M. W. Dunlop, A. Roux, and G. Chanteur (1998), Accuracy of current density determination, in *Analysis Methods for Multi-spacecraft Data*, edited by G. Paschmann and P. W. Daly, pp. 395–418, ESA Publ., Noordwijk, Netherlands.

Rong, Z. J., W. X. Wan, C. Shen, X. Li, M. W. Dunlop, A. A. Petrukovich, T. L. Zhang, and E. Lucek (2011), Statistical survey on the magnetic structure in magnetotail current sheets, *J. Geophys. Res.*, *116*, A09218, doi:10.1029/2011JA016489.

Russell, C. T., M. M. Mellott, E. J. Smith, and J. H. King (1983), Multiple spacecraft observations of interplanetary shocks: Four spacecraft determination of shock normals, *J. Geophys. Res.*, *88*, 4739–4748, doi:10.1029/JA088iA06p04739.

Russell, C. T., et al. (2015), The magnetospheric multiscale magnetometers, *Space Sci. Rev.*, doi:10.1007/s11214-014-0057-3.

Sergeev, V. A., E. M. Sazhina, N. A. Tsyganenko, J. A. Lundblad, and F. Soraas (1983), Pitch-angle scattering of energetic protons in the magnetotail current sheet as the dominant source of their isotropic precipitation into the ionosphere, *Planet. Space Sci.*, *31*, 1147.

Shen, C., X. Li, M. Dunlop, Z. X. Liu, A. Balogh, D. N. Baker, M. Hapgood, and X. Wang (2003), Analyses on the geometrical structure of magnetic field in the current sheet based on cluster measurements, *J. Geophys. Res.*, *108*(A5), 1168, doi:10.1029/2002JA009612.

Shen, C., et al. (2008), Flattened current sheet and its evolution in substorms, *J. Geophys. Res.*, *113*, A07S21, doi:10.1029/2007JA012812.

Shen, C., et al. (2014), Direct calculation of the ring current distribution and magnetic structure seen by Cluster during geomagnetic storms, *J. Geophys. Res. Space Physics*, *119*, 2458–2465, doi:10.1002/2013JA019460.

Sonnerup, B. U. Ö., and M. Scheible (1998), Minimum and maximum variance analysis, in *Analysis Methods for Multi-spacecraft Data*, edited by G. Paschmann and P. W. Daly, chap. 8, pp. 185–220, ESA Publ., Noordwijk, Netherlands.

Speiser, T. W. (1965), Particle trajectories in a model current sheet, based on the open model of the magnetosphere, with applications to auroral particles, *J. Geophys. Res.*, *70*, 1717–1728, doi:10.1029/JZ070i007p01717.

Wan, W. G., G. Lapenta, G. L. Delzanno, and J. Egedal (2008), Electron acceleration during guild field magnetic reconnection, *Phys. Plasmas*, *15*, 032903.

Wang, R., Q. Lu, C. Huang, and S. Wang (2010), Multi spacecraft observation of electron pitch angle distributions in magnetotail reconnection, *J. Geophys. Res.*, *115*, A01209, doi:10.1029/2009JA014553.

Wang, S., L.-J. Chen, N. Bessho, L. M. Kistler, J. R. Shuster, and R. Guo (2016), Electron heating in the exhaust of magnetic reconnection with negligible guide field, *J. Geophys. Res. Space Physics*, *121*, doi:10.1002/2015JA021892.

Yang, Y. Y., C. Shen, Y. C. Zhang, Z. J. Rong, X. Li, M. Dunlop, Y. H. Ma, Z. X. Liu, C. M. Carr, and H. Rème (2014), The force-free configuration of flux ropes in geomagnetotail: Cluster observations, *J. Geophys. Res. Space Physics*, *119*, 6327–6341, doi:10.1002/2013JA019642.

Young, S. L., R. E. Denton, B. J. Anderson, and M. K. Hudson (2008), Magnetic field line curvature induced pitch angle diffusion in the inner magnetosphere, *J. Geophys. Res.*, *113*, A03210, doi:10.1029/2006JA012133.

Zhang, Y. C., et al. (2013), Two different types of plasmoids in the plasma sheet: Cluster multisatellite analysis application, *J. Geophys. Res. Space Physics*, *118*, 5437–5444, doi:10.1002/jgra.50542.

Zou H., Q.-G. Zong, G. K. Parks, Z. Pu, H.-F. Chen, and L. Xie (2011), Response of high-energy protons of the inner radiation belt to large magnetic storms, *J. Geophys. Res.*, *116*, A10229, doi:10.1029/2011JA016733.